Eddy Generation by Flow Over Variable Topography: Some Experiments

Christopher L. Wolfe

1 Introduction

The Labrador Sea is a marginal sea of the North Atlantic Ocean bounded by Canada on the west and Greenland on the east. The prevailing winds are from the west and, in the winter, very cold and dry. The surface waters of the Labrador Sea are typically warmer and salter than the water at depth. In severe weather, the sensible and latent heat fluxes can be sufficient to render the surface water denser than the water below. Convective overturning ensues that can mix the water column to depths of over 2 kilometers, creating an intermediate mode water known as Labrador Sea Water[1].

The Labrador Sea Water that forms in these deep convective events spreads out at depth and forms part of the driving force for the global thermohaline circulation whereby dense water formed at high latitudes spreads throughout the world oceans, upwells and warms, and returns to the polar oceans. This circulation transports a large amount of heat from the topics to the poles and is important for maintaining a temperate climate at high latitudes. The deep convection driving this circulation occurs only in a few isolated locations in the arctic and antarctic and an understanding the dynamics of these areas is essential to an understanding of the world climate.

After winters of intense convection, the newly formed Labrador Sea Water is rapidly capped by a thick layer of stratified water. There are too few observations of the restratification process to provide a clear picture of its mechanism, but it is too rapid to be driven simply by surface warming at the beginning of spring. This suggests that horizontal fluxes driven by eddies may be responsible. A possible source of warm, fresh water is eddies shed by the Irminger Current—a fresh, buoyancy driven boundary current rimming the Labrador Sea. West of Greenland the continental shelf is narrower and the continental slope steeper than along the rest of the coast, and the most intense region of eddy formation is at the downstream end of this constriction[1]. A modeling study by Katsman *et al.*[2] indicate that Irminger Current eddies are triggered by rapid variations in shelf topography. In particular, they showed that narrow alongshelf gaps were less effective at generating eddies than large gaps, and that topography with abrupt transitions generates eddies more efficiently than gently varying topography.

The stability of a buoyant boundary current flowing along topography which does not vary in the downstream direction is a hard enough problem, for which there are few general

theoretical results. A necessary condition for baroclinic instability of a two layer flow is known, namely that the gradient of the potential vorticity (PV),

$$\Pi = \frac{\zeta + f}{h} \quad \text{where} \quad \zeta = (\nabla \times \boldsymbol{u}) \cdot \hat{\mathbf{k}}, \tag{1}$$

must change signs somewhere in the flow (see, for example, [3]). If the PV gradient is of a single sign in each layer, this condition implies that the PV gradient in the upper layer must be of opposite sign as the PV gradient in the lower layer for instability to occur. Simple application of this condition shows that bottom topography that slopes in the same direction as a front can render the front completely baroclinically stable[4]. Topography that slopes in the opposite direction can be destabilizing, but there are many instances of currents flowing over topography with a 'destabilizing' (i.e. opposing) slope that are nevertheless stable[5, 6, 7].

Several authors have studied the stability of fronts over sloping topography in specific situations. Flagg and Beardsley[8] and Gawarkiewicz[9] investigated the linear stability of surface to bottom shelfbreak fronts over topography that slopes away from the front. They find that the front is unstable for any slope, but is most unstable over gentle slopes, becoming rapidly more stable for very steep slopes. The stability of a surface trapped front over sloping topography was studied by Reszka and Swaters[10] using a nonlinear numerical model based on an asymptotic expansion of the primitive equations that assumes that the ratio of the upper layer depth to the lower layer depth is small. They also find that an opposing slope is destabilizing, but that the front becomes less stable as the slope is increased. The very different mean frontal structures (surface to bottom verses surface trapped) may be a source of the discrepancy between these two sets of studies.

The effect of rapidly varying topography on the stability of buoyant currents is less well studied. Bracco and Pedlosky[11], building on a study by Samelson and Pedlosky[12], investigated the stability of a two-layer, quasi-geostrophic channel model with topographic variations in the along-channel direction. The flow in the bulk of the channel was stabilized by a bottom that sloped in the same direction as the interface between the two layers. The slope was smoothly reduced to zero in a narrow gap, thus inducing instability in the gap. They found that the gap strongly influenced the flow downstream of the gap; in their nonlinear model this influence was in the form of coherent vortices that formed in the gap and propagated downstream. These vortices formed and propagated for arbitrarily narrow gaps, contrary to the naive expectation that a gap narrower than one Rossby radius of deformation should have no effect on the flow. The authors suggest that their model could be a possible model for the formation of eddies in the Irminger Current. However, the restriction to small interface deflections (required by quasi-geostrophy) and a bottom that slopes in the same direction as the front (opposite to that of a shelfbreak front) makes the application of this model to the Irminger Current problematic.

We performed a series of laboratory experiments in order to better understand the effect of variable topography on buoyant coastal currents. In order to determine the stability characteristics of a buoyant current on a single slope, we performed a set of preliminary experiments in which the input parameters were varied over a large range. We then allowed the current to flow from a slope which was known to be stable to an unstable slope, or from a slope which was unstable to a slope which was stable. Finally, we attempted to simulate

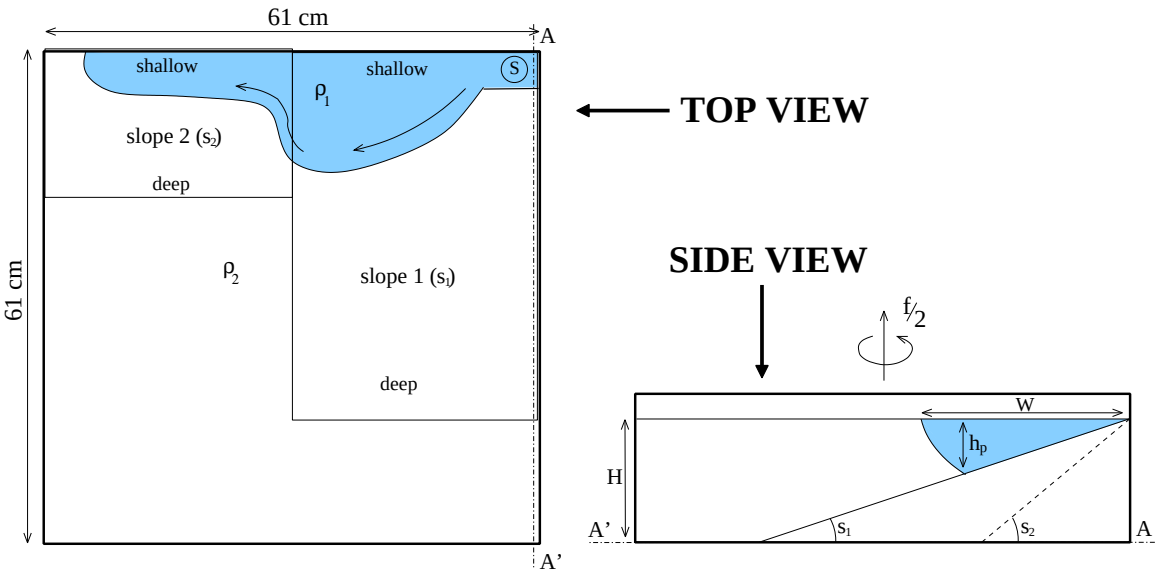

Figure 1: Experimental apparatus used in the preliminary experiments. Left: top view, Right: side view. The arrows indicate the flow direction.

the Irminger Current west of Greenland by allowing the current to flow over two identical, stable slopes separated by a variable width gap containing an unstable slope.

The format of the paper is as follows: In section 2, we will describe the experimental methods. Section 3 will introduce some theoretical results pertaining to buoyant coastal currents. In sections 4 and 5 we discuss the qualitative and quantitative results, respectively, of the experiments. Finally, we conclude in section 6.

2 Experimental Methods

The experiments were performed in three phases, using three different experimental apparatuses. The three phases will be referred to as the preliminary, two-slope, and gap experiments, respectively.

A sketch of the apparatus used in the preliminary experiments is shown in figure 1. These experiments were conducted in a transparent plastic tank of depth 60 cm with a square base measuring 61 cm on a side. The tank was mounted on a 1 meter diameter, belt-driven, rotating table with a vertical axis of rotation. The tank was filled with salt water of density ρ_2 to a depth of about 15 cm. The right 30 cm (in the frame of figure 1) of the tank had a bottom with slope s_1, with the fluid shallowest toward the top of the figure. The left 30 cm had a sloping bottom with slope $s_2 \neq s_1$, again with fluid shallowest toward the top of the figure. The level of water in the tank was adjusted so that the two slopes intersected at the free surface. Dyed buoyant water of density $\rho_1 < \rho_2$ flowed from the 1.1 cm diameter nozzle (marked 'S' in the figure) placed about 0.5 cm below the free surface. The nozzle was covered with a piece of sponge to reduce mixing between the buoyant and ambient fluids. The buoyant water flowed onto the right-hand slope where it developed into a buoyancy forced boundary current which flowed with the coast on its right

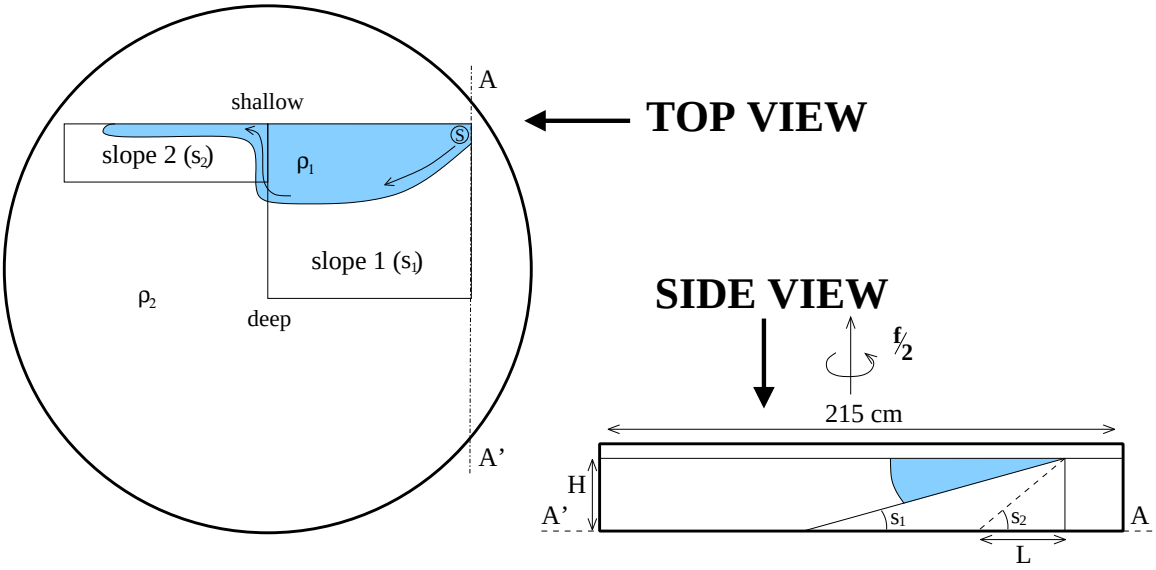

Figure 2: Experimental apparatus used in the two-slope experiments. Left: top view, Right: side view. The arrows indicate the flow direction.

(looking downstream) before flowing onto the left-hand slope. In this arrangement, buoyant fluid could flow all the way around the tank and rejoin the current near the source. The experiment was ended before this happened.

In all that follows, the first slope that the buoyant fluid encounters will be referred to as slope 1 and the other slope is slope 2. The buoyancy force on the current is described by the reduced gravity $g' = g(\rho_2 - \rho_1)/\bar{\rho}$, where g is the gravitational acceleration and $\bar{\rho} = (\rho_2 + \rho_1)/2$. The reduced gravity was calculated using the densities of the fluids before the beginning of the experiment; the actual value was reduced somewhat by mixing. Sampling of buoyant water from developed current revealed that g' was reduced in the experiments by between 20% and 50%. In the first set of experiments $s_1 = 0.25$ or 0.30 and $s_2 = 0.79$ or ∞ (a vertical wall). For the preliminary experiments, the other parameters were varied greatly to explore a large region of parameter space. The Coriolis parameter f varied from 0.20 s^{-1} to 3.0 s^{-1} and the reduced gravity g' took on values from 0.40 cm/s^2 to 12 cm/s^2. The flow rate Q was varied from 0.75 cm^3/s to 18 cm^3/s.

The two-slope experiments (shown in figure 2) were performed in a 215 cm diameter, 45 cm deep, opaque plastic tank mounted on a 2 meter diameter, direct-drive rotating table with a vertical axis of rotation. The tank was filled to a depth of either $H = 15$ cm or $H = 22.5$ cm with salt water of density ρ_2. The two slopes where mounted in the tank away from the side walls. The lengths of the first and second slopes were 72 cm and 82 cm, respectively, and both slopes were painted with a 10 cm by 10 cm grid. The first slope was fixed with $s_1 = 0.29$ while the second slope was adjustable from $s_2 = 1.0$ to $s_2 = \infty$. The source of buoyant fluid as well as the progress of the experiments is the same as that described above. However, since the slopes were mounted away from the side walls of the tank, the buoyant fluid could not make a circuit of the tank and rejoin the current near the source. This allowed us to run the experiment until our reserves (about 20 liters) of

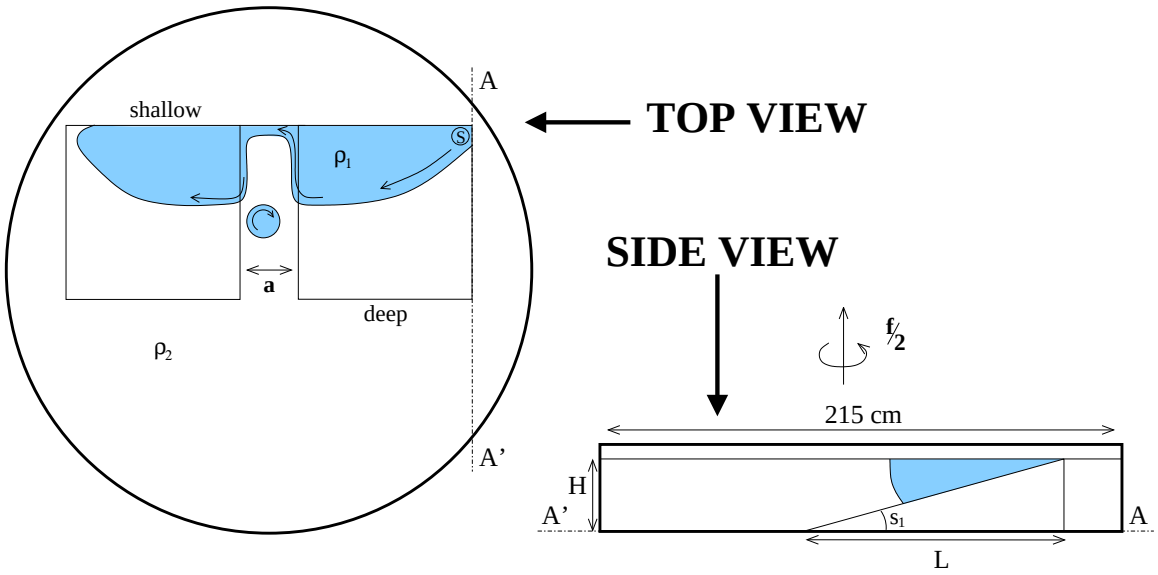

Figure 3: Experimental apparatus used in the gap experiments. Left: top view, Right: side view. The arrows indicate the flow direction. The isolated circle of buoyant fluid represents an eddy which often forms in the gap.

buoyant fluid were depleted. For several experiments, we wanted the current to start on a steep slope and flow onto the gentle slope. Rather than physically reverse the position of the slopes, we simply moved the source to the left end of the left-hand slope and spun the table anti-clockwise. The current then flowed from left to right, with the coast on the left (looking downstream). In all the two-slope experiments, the reduced gravity was kept fixed at $g' \approx 1$ cm/s^2, except for four experiments where $g' \approx 13$ cm/s^2. The magnitude of the Coriolis parameter $|f|$ varied from 0.5 s^{-1} to 2.0 s^{-1}, but was usually fixed at $|f| = 2.0$ s^{-1}. The flow rate was fixed at $Q = 12$ cm^3/s, except for one experiment where $Q = 6.0$ cm^3/s.

The gap experiments (shown in figure 3), where performed in the same tank as the two-slope experiments using two identical slopes with slope $s = 0.29$ separated by a gap of width a. The shoreward side of the gap was a vertical wall. In all other respects, these experiments were identical to the two-slope experiments. The gap width a took on values of 1 cm, 5 cm, 10 cm, 20 cm, and 40 cm. All other parameters were kept fixed with $g' = 1$ cm/s^2, $f = 2.0$ s^{-1}, and $Q = 12$ cm^3/s.

For all of the above experiments, data was captured using a video camera which was co-rotating with the table. The current was made visible by the addition of food coloring and, in several experiments, surface velocities were visualized by floating paper pellets on the surface. The gap experiments were additionally visualized using potassium permanganate dye crystals. The width of the current was determined as the average of three measurements separated by 20 cm, starting at 20 cm downstream from the source on slope 1 or 20 cm downstream from the joint between the two slopes on slope 2.

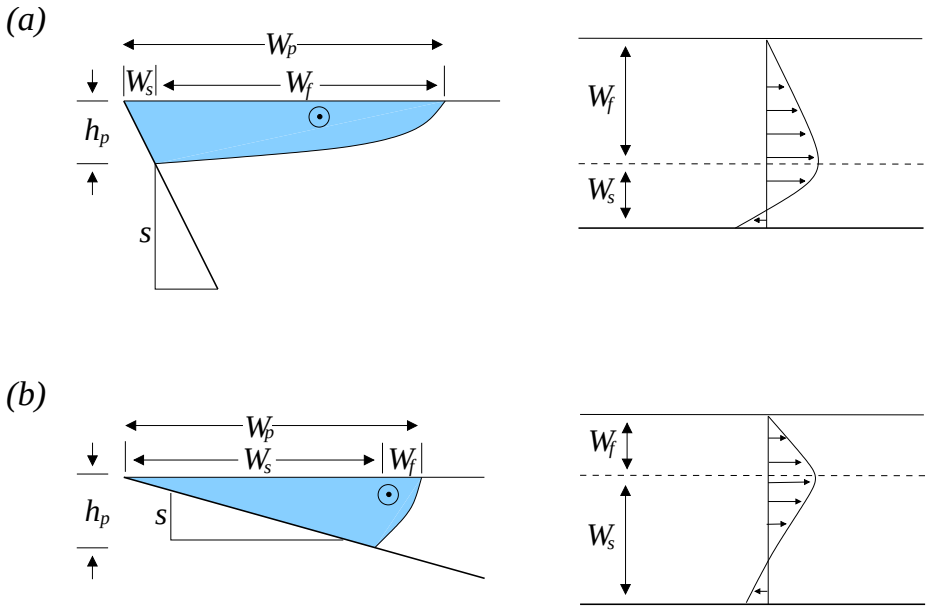

Figure 4: Basic structure of a buoyant current over a sloping bottom, cross-section on the left and plan view on the right. (a) Surface trapped front. (b) Bottom trapped front.

3 Scaling for Buoyant Boundary Currents

Lentz and Helfrich[13] introduced and tested a scaling theory for buoyant currents flowing over a sloping bottom in a rotating fluid. The basic structure of a buoyant current over a sloping bottom is shown in figure 4. The buoyant fluid occupies the entire water column in a wedge of width W_s and depth h_p. Offshore of this point, the front detaches from the bottom and curves upward to meet the surface at a distance W_p offshore. The point where the front intersects the bottom is called the foot of the front and the distance from the foot to the seaward edge of the front will be referred to as W_f.

We assume throughout that the front is quasi-steady and in geostrophic and hydrostatic balance. If we also assume that the free surface deformation and the viscous forces are small then the wedge shoreward of the foot is quiescent, while the dynamics seaward of the foot are governed by

$$-fv = -g'h_x \tag{2}$$

where v is the along-shelf velocity, h is the depth of the interface between the buoyant and dense water, and subscripts stand for partial differentiation. The position of the foot is fixed by requiring that the current transport a known flux Q, since

$$Q = \int_0^{W_p} vh\,dx = \frac{f}{2g'}\int_{W_s}^{W_p} (h^2)_x\,dx = \frac{fh_p^2}{2g'}, \tag{3}$$

so

$$h_p = \sqrt{\frac{2Qf}{g'}}. \tag{4}$$

The offshore position of the foot, then, is $W_s = h_p/s$. In fact, the foot is 'trapped' at this position[14] since this is exactly the position at which the vertically sheared, geostrophic velocity is zero at the bottom. If the front were to move toward shore, a negative geostrophic velocity would develop at the bottom. The resulting offshore Ekman flux in the bottom boundary layer would force the foot back offshore. Conversely, if the front moves offshore, a positive geostrophic velocity at the bottom would drive an Ekman flux onshore, forcing the foot back to its trapping depth. In practice, there is always some downstream transport shoreward of the foot driven, perhaps, by alongshore pressure gradients. This will lead to a somewhat reduced value of h_p and, hence, W_s.

The offshore portion of the front is assumed to initially adjust to a width of one Rossby radius based on the depth of the foot:

$$W_f(0) \sim L_R = \frac{\sqrt{g'h_p}}{f}, \tag{5}$$

giving an initial mean frontal slope and velocity of

$$s'_0 = \frac{h_p}{W_f(0)} = \frac{h_p}{L_R} \qquad\qquad v_0 = \frac{s'g'}{f} \sim \sqrt{g'h_p}. \tag{6}$$

The total width of the current is then

$$W_p = W_s + W_f(0). \tag{7}$$

The ambient fluid is assumed to be quiescent and the shear between the buoyant and ambient fluids is assumed to be concentrated at the interface between the layers. This shear produces drag on the moving layer which creates an interfacial Ekman layer that transports buoyant water offshore, causing the front to spread slowly. Assuming that the spreading rate is equal to the average offshore velocity in the interfacial Ekman layer,

$$\frac{\partial W_f(t)}{\partial t} \sim u_E = \frac{v}{4} = \frac{fL_R^2}{4W_f}, \tag{8}$$

we find that

$$W_f(t) \sim L_R \left(\frac{tf}{2}\right)^{1/2}. \tag{9}$$

This equation holds for times long compared to the initial adjustment of the front to its trapping depth. In terms of the total current width $W = W_s + W_f$, normalized by the width W_p given by equation (7),

$$\frac{W}{W_p} = \left(\frac{t}{2t_p}\right)^{1/2} + \frac{s'/s}{1 + s'/s}, \tag{10}$$

where $t_p = (1 + s'/s)/f$. The current will continue to spread until a diffusive boundary layer of thickness greater than an Ekman thickness develops between the layers. This will halt the interfacial Ekman transport and shut down the spreading of the current.

The parameter s'/s which appears above is an important parameter for predicting the behavior of a current over sloping topography. If $s'/s \gg 1$ the current is 'bottom trapped'

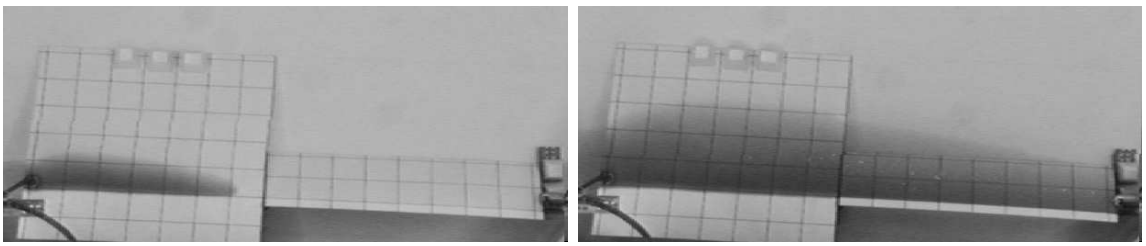

Figure 5: Evolution of a surface trapped front ($Q = 12.0$ cm^3/s, $f = 2.0$ s^{-1}, $g' = 13.2$ cm/s^2, $s_1 = 0.29$, $s_2 = 1.0$, $s' = 0.14$) after 12 s (left) and 144 s (right).

(figure 4b) and if $s'/s \ll 1$ the current is 'surface trapped' (figure 4a), using the terminology of Yankovsky and Chapman[15]. Bottom trapped currents are strongly controlled by bottom topography whereas surface trapped currents are only mildly so.

Lentz and Helfrich[13] performed a number of laboratory experiments to test this scaling theory. They found the width and spreading rates of the current to be well predicted if they take the trapping depth $h \approx (0.7 \pm 0.1)h_p$.

4 Qualitative Results

In all the experiments performed, buoyant water spread from the source and flowed along the coast with the coast on the right looking downstream (for positive f). The current broadened rapidly as it flowed away from the source and equilibrated to a width similar to that predicted by Lentz and Helfrich[13] about 20 cm downstream of the source. The foot of the current was visible as a maximum in dye intensity, but it was not feasible to measure its position accurately. After the initial equilibration, the current continued to widen slowly, possibly due to interfacial drag, occasionally forming filamentous streamers on the seaward edge due to offshore transport in the surface Ekman layer. When these occurred the width of the current was measured with the streamers excluded.

During the preliminary experiments, we varied all the input parameters over a wide range to characterize the stability of the current along a slope or a wall. Over the range of parameters used, the current was always stable on the gentle slope. It was found that a fairly large value of $s' > 3$ was needed to generate instabilities along a vertical wall within the time scale of the experiment and that flows over sloping topography were always more stable that flows along a vertical wall.

4.1 Two-Slope Experiments

4.1.1 Surface Trapped, Gentle to Steep

We performed five experiments with relatively high reduced gravities and low rotation rates in order to make a close comparison with the results of Lentz and Helfrich[13]. These flows are predominately surface trapped, with $s'/s \approx 0.3$–1.0. All of these experiments had the source located over gentle topography with steeper topography placed downstream. As expected for surface trapped flows, the topography did not greatly influence the evolution

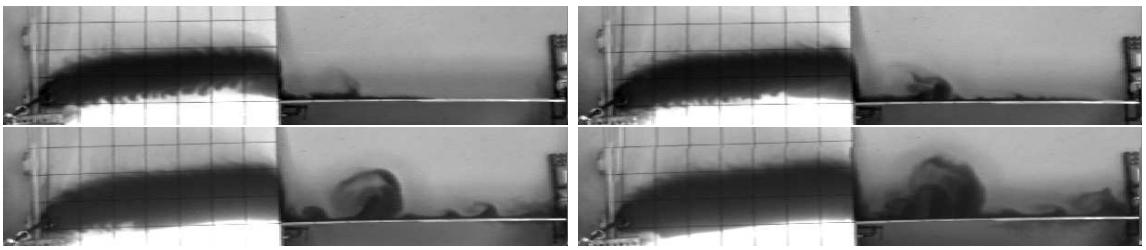

Figure 6: A bottom trapped front ($Q = 12.0$ cm^3/s, $f = 2.0$ s^{-1}, $g' = 0.78$ cm/s^2, $s_1 = 0.29$, $s_2 = \infty$, $s' = 6.1$) flowing from a gentle slope to a vertical wall after 240 s (upper left), 288 s (upper right), 408 s (lower left), and 504 s (lower right). Note the immediate formation of a large eddy on the vertical wall.

of the current. The evolution of a surface trapped front is shown in figure 5. The current propagated quickly across both slopes and was stable throughout the entire experiment. The width of the current decreased slightly on slope 2, but the current was otherwise unaffected by the change in topography. Aside from presence of two slopes, this figure is virtually indistinguishable from figure 5 in Lentz and Helfrich[13].

4.1.2 Bottom Trapped, Gentle to Steep

The bottom trapped currents evolved much more slowly than the surface trapped currents and their cross-shelf extent was smaller, with an equilibrated width on slope 1 rarely greater than 25 cm. Do to their slow spreading, these currents often trapped some dense ambient water between the current and the coast. This density contrast drove a flow along the shoreward edge of the current that was *upstream* relative to the mean flow of the current. The shoreward front was extremely susceptible to instabilities which tended to smooth out the edge of the front. These instabilities are visible in the first two panels of figure 6. However, no eddies were observed to form on the seaward edge of the front when the current flowed over a gentle slope.

When the nose of the current passed from the gentle to the steep slope, it often formed a wisp of fluid (visible in the first panel of figure 6) extending into the ambient fluid. This wisp may be caused by entrainment of buoyant fluid in a cyclonic eddy of ambient fluid formed when the current flows from the gentle to the steeply sloping topography. This initial perturbation propagated more slowly than the nose of the current and decayed downstream over all topography with less than a vertical slope. When the current flowed along a vertical wall, this perturbation grew rapidly into a large eddy. This eddy consumed much of the flux along the wall and delayed the formation of further instabilities downstream of the eddy. Other instabilities eventually grew and formed eddies, the beginnings of which are seen in the last two panels of figure 6. Immediate formation of a large eddy seemed to be a particular feature of flow onto a vertical wall and was not observed for large but finite slopes.

When the current flowed from a gentle slope to a steep—but not vertical—slope the initial perturbation died out before it could grow to a large amplitude eddy. The flow along the steep slope was initially steady and laminar. As the experiment progressed the current

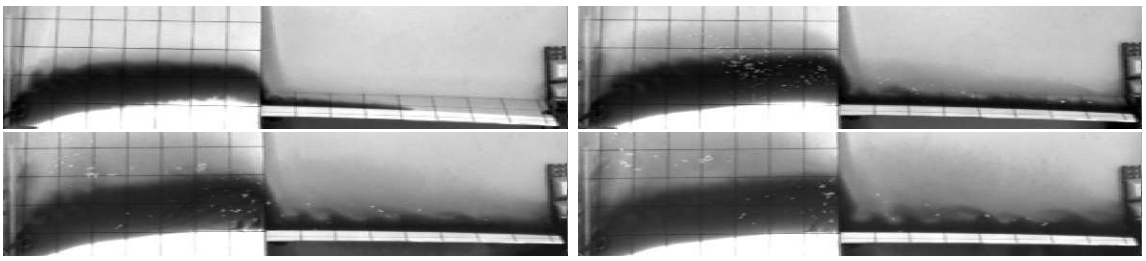

Figure 7: A bottom trapped front ($Q = 12.0$ cm^3/s, $f = 2.0$ s^{-1}, $g' = 1.0$ cm/s^2, $s_1 = 0.29$, $s_2 = 3.7$, $s' = 5.3$) flowing from a gentle slope to a steep slope after 124 s (upper left), 279 s (upper right), 465 s (lower left), and 589 s (lower right).

widened and occasionally developed meanders, but the development of large scale eddies was delayed until the current was wider than the sloping shelf and the seaward edge of the current lay over the flat bottom. An example of this behavior can be seen in figure 7. This behavior was observed on all slopes with $s > 1$. This lead us to believe that fully developed eddies cannot form over strongly sloping topography and that the current must be sufficiently wide so as to extend beyond edge of the sloping topography before eddies can form.

In order to test this idea, we performed a series of experiments where the depth of the ambient fluid was increased to 22.5 cm from 15.0 cm, but the slopes were unchanged. This increased the width of the sloping shelf without changing its steepness. In these experiments, the formation of eddies was again delayed until the current extended beyond the shelf and the seaward edge of the current lay over the flat bottom.

The detailed evolution of all currents that formed eddies over steep topography is shown in figure 8, showing that eddies only form once the current is wider than the shelf. In fact, in all cases the current was wider than the shelf by almost a factor of two before eddies formed. Another way to see this is to plot the width of the current when eddies start forming verses with width of the shelf. This is shown in figure 9 where, in addition, the width of the current at the end of the experiment has been plotted versus the width of the shelf for all experiments. Again, all of the eddying currents fall above the line $W = L$. Five currents that were steady at the end of the experiment also lie above the line $W = L$. These experiments were the surface trapped experiments discussed in section 4.1.1. These currents were stable under any condition tested.

4.1.3 Bottom Trapped, Steep to Gentle

We can also inquire as to what will happen if a flow which is initially unsteady and eddying is allowed to flow onto a gentle slope. We have observed that currents starting on gentle slope never form eddies, but it was not clear whether this was a result of a special initial condition or a general statement about the stability of currents over slopes. Figure 10 shows the evolution of a current flowing from a steep slope onto a gentle slope. The current was initially laminar on both slopes, but formed eddies once the current width on slope 1 exceeded the width of the shelf. Regardless of how unstable the current was on slope 1 it was immediately stabilized once it flowed onto slope 2. Eddies formed on slope 1 evidently

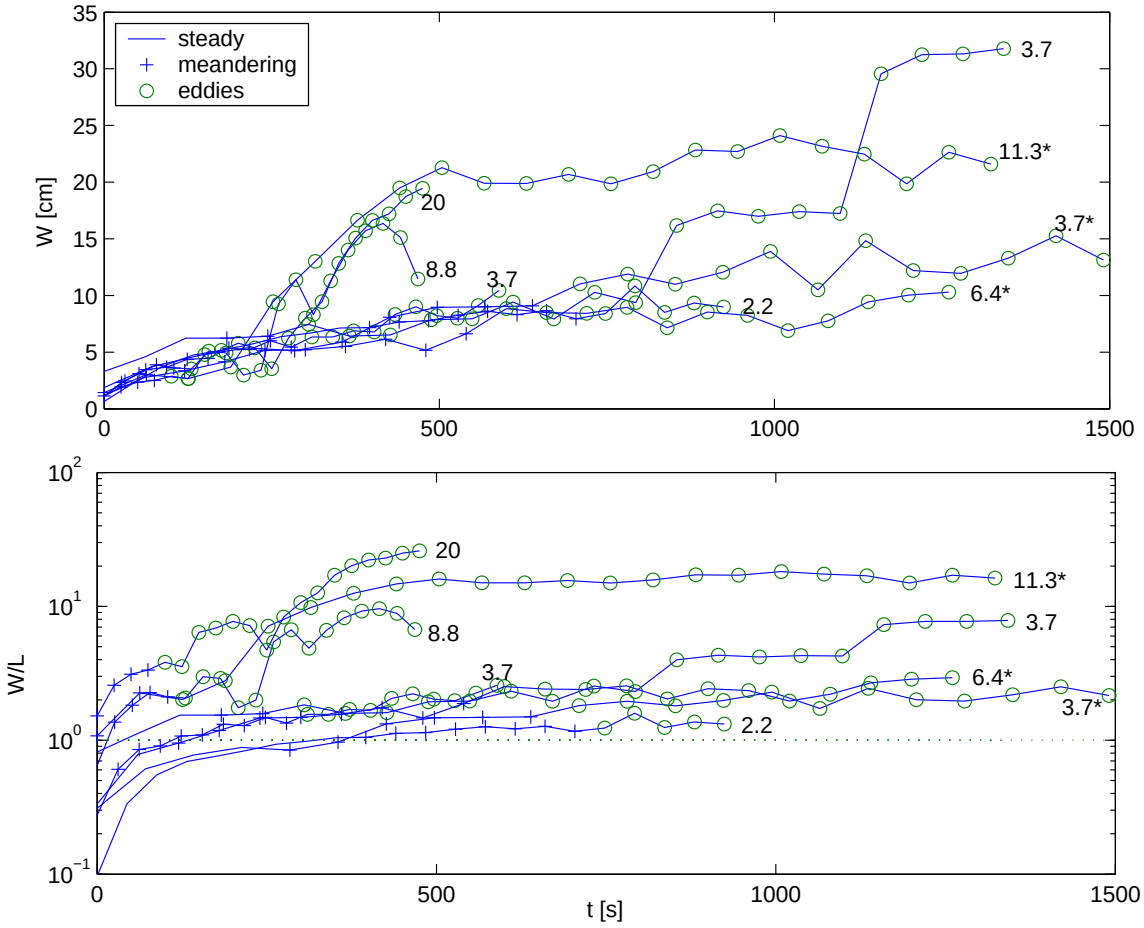

Figure 8: The total width verses time for currents on a slope that eventually formed eddies. '+'s and 'o's indicate that the current is meandering or forming eddies, respectively. Numbers at the end of each curve give the slope over which each current formed. Those with asterisks have total depth $H = 22.5$ cm, those without have $H = 15.0$ cm. Top: Total width W. Bottom: Total width normalized by the width of the shelf $L = H/s$.

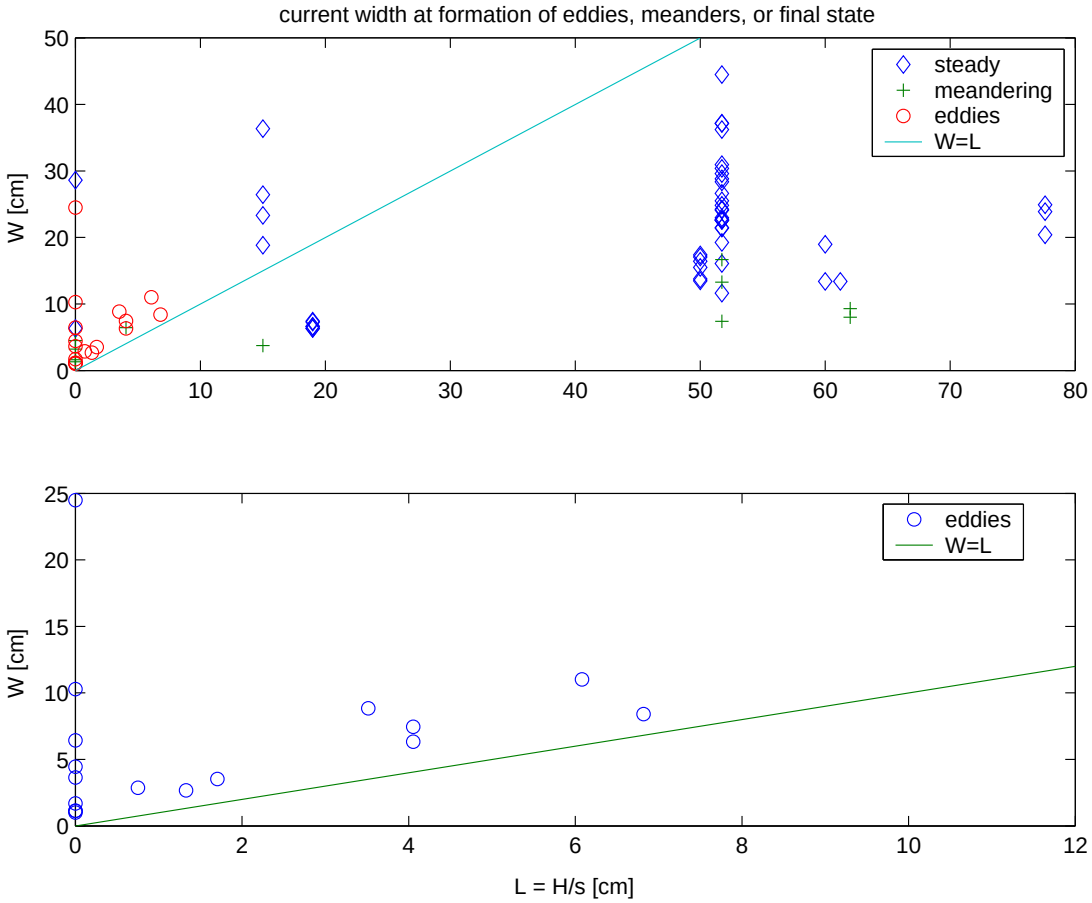

Figure 9: Final width of current verses shelf width $L = H/s$ for all experiments (upper panel) and only currents that form eddies (lower panel). For currents that form eddies, the final width was measured just before eddies began to form.

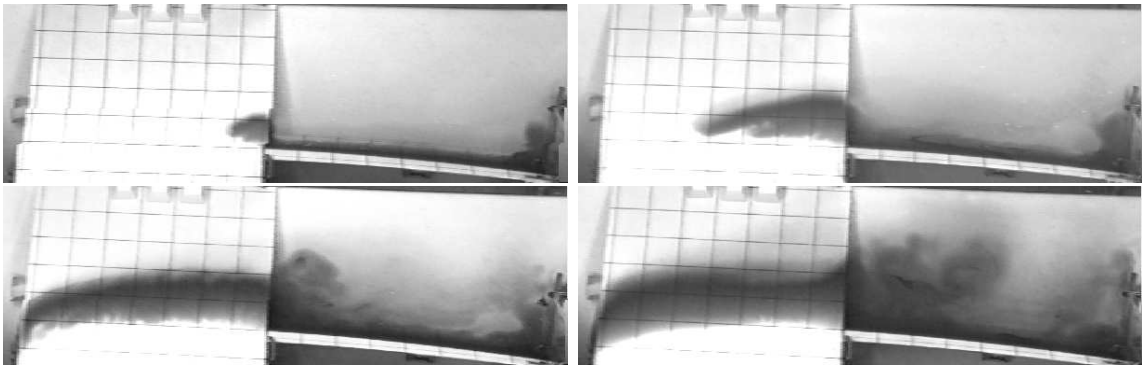

Figure 10: A bottom trapped front ($Q = 12.0$ cm^3/s, $f = -2.0$ s^{-1}, $g' = 1.0$ cm/s^2, $s_1 = 3.7$, $s_2 = 0.29$, $s' = 5.3$) flowing from a steep slope to a gentle slope after 122 s (upper left), 305 s (upper right), 610 s (lower left), and 1037 s (lower right). Note that the current flows from right to left since f is negative.

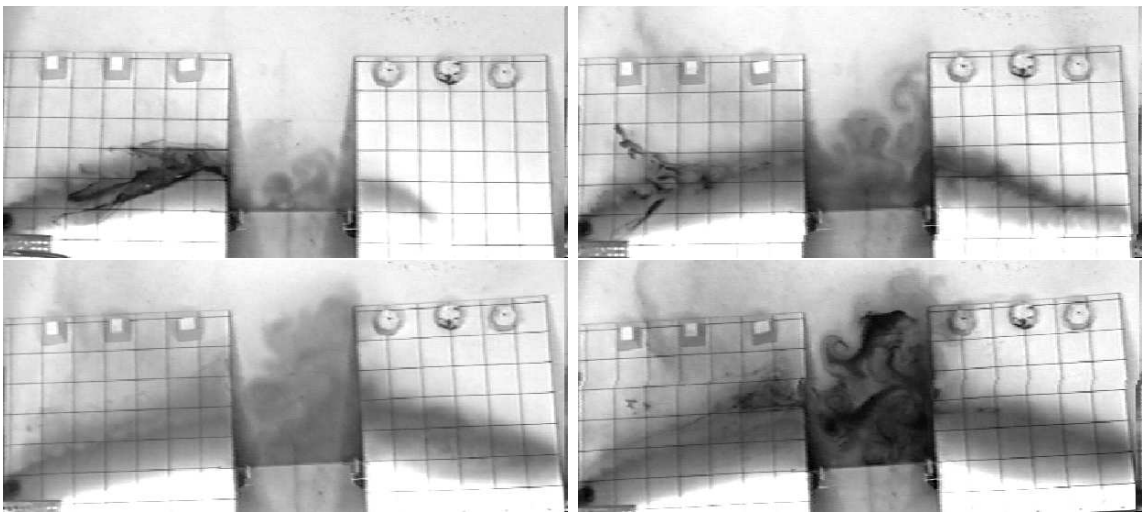

Figure 11: A bottom trapped front ($Q = 12.0$ cm^3/s, $f = 2.0$ s^{-1}, $g' = 1.0$ cm/s^2, $s_1 = 0.29$, $s_2 = 0.29$, $s' = 5.3$, $a = 40$ cm) flowing across a gap after 372 s (upper left), 837 s (upper right), 1302 s (lower left), and 1767 s (lower right). Darker dye was occasionally injected to help visualized the flow field. Note that the eddies pile up at the downstream edge of the gap.

could not propagate onto slope 2 and piled up at the upstream edge of the slope. This behavior is similar to the behavior of Irminger Current eddies formed in the constriction west of Greenland (see Katsman *et al.*[2] figure 1).

4.2 Gap Experiments

The gap experiments were performed with gap sizes ranging from $a = 1$ cm to $a = 40$ cm, corresponding to $a = 0.8L_R$ to $a = 32L_R$, where L_R is the Rossby radius of deformation given by equation (5). For experiments with $a \leq 4L_R$ the flow exhibited small perturbations that decayed downstream of the gap, but no eddies were observed to form.

Once the gap size was increased to $a = 8L_R$, eddies began to form in the gap. It should be noted that the smallest fully developed eddies observed in the previous experiments had diameter $D \approx 8L_R$. Thus, eddies were unable to form in the gap until the gap was wide enough to contain a least one fully developed eddy. Two coherent eddies formed in the gap when $a = 8L_R$: a cyclonic eddy of ambient fluid near the wall and an anticyclonic eddy of buoyant fluid seaward of the first eddy. When the gap was increased to $a = 16L_R$ three eddies formed, with a cyclonic/anticyclonic pair occupying the same positions as before and an additional cyclonic eddy seaward of the anticyclonic eddy. The first two eddies were stationary throughout the experiment, while the third eddy migrated back and forth across the gap, sometimes closer to slope 1, at other times closer to slope 2. The experiment with the largest gap ($a = 32L_R$, shown in figure 11) developed at random eddy field where the number of eddies increased as the experiment proceeded. By the end of the experiment, at least seven individual eddies and dipoles had formed. A summary of the gap experiments is shown in figure 12.

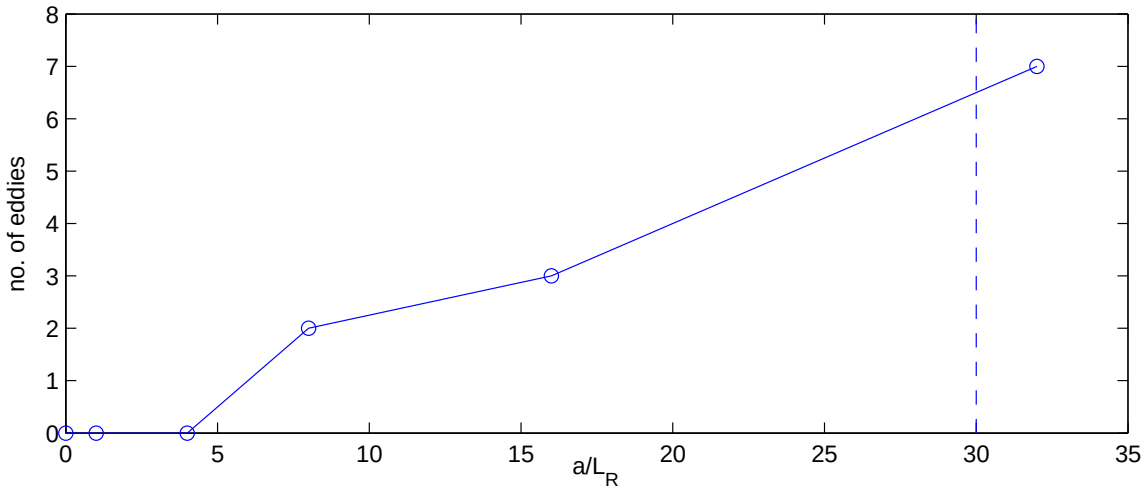

Figure 12: Number of eddies observed in gap experiments verses gap width in Rossby radii. The dashed line represents a lower bound on the width of the constriction associated with Irminger Current eddies.

In none of the gap experiments were eddies that formed in the gap able to propagate onto the gentle slopes, either upstream or downstream of the gap. Eddies advected downstream in the gap accumulated on the downstream edge of the gap rather than propagating onto the slope, as in figure 11.

5 Quantitative Results

If time and the width of the current are scaled as discussed in section 3, the data should collapse onto a set of curves with time dependence like $t^{1/2}$. Equation (10) places a bound on the expected variation of the data if bounds on s'/s are known. If the data is scaled using the value of h_p given by equation (4), it does not collapse onto a single curve well and does not fit within the required bounds. As noted in section 3, the observed value of the trapping depth h often falls short of the predicted value h_p. Using $h = h_p/2$ (shown in figure 13) produces a scaling which collapses the data and causes it fall within the required bounds reasonably well for the first slope. However, the width of the current on the second slope consistently falls short of the predicted width. This shortfall may be caused by a reduction in Q caused by upstream flow on the shoreward edge of the front (discussed in section 4.1.2).

An estimate of the growth rate of disturbances on the current can be found by measuring the growth of the current once it begins to meander. If we assume the growth rate of the disturbance is much larger than the spreading rate due to interfacial drag, then the mean growth rate of the disturbances is simply the growth of the current divided by the time it takes the current to grow:

$$\sigma = \frac{W_f - W_i}{W_i \Delta t}, \tag{11}$$

where W_i and W_f are the initial and final widths of the current, respectively. Figure 14

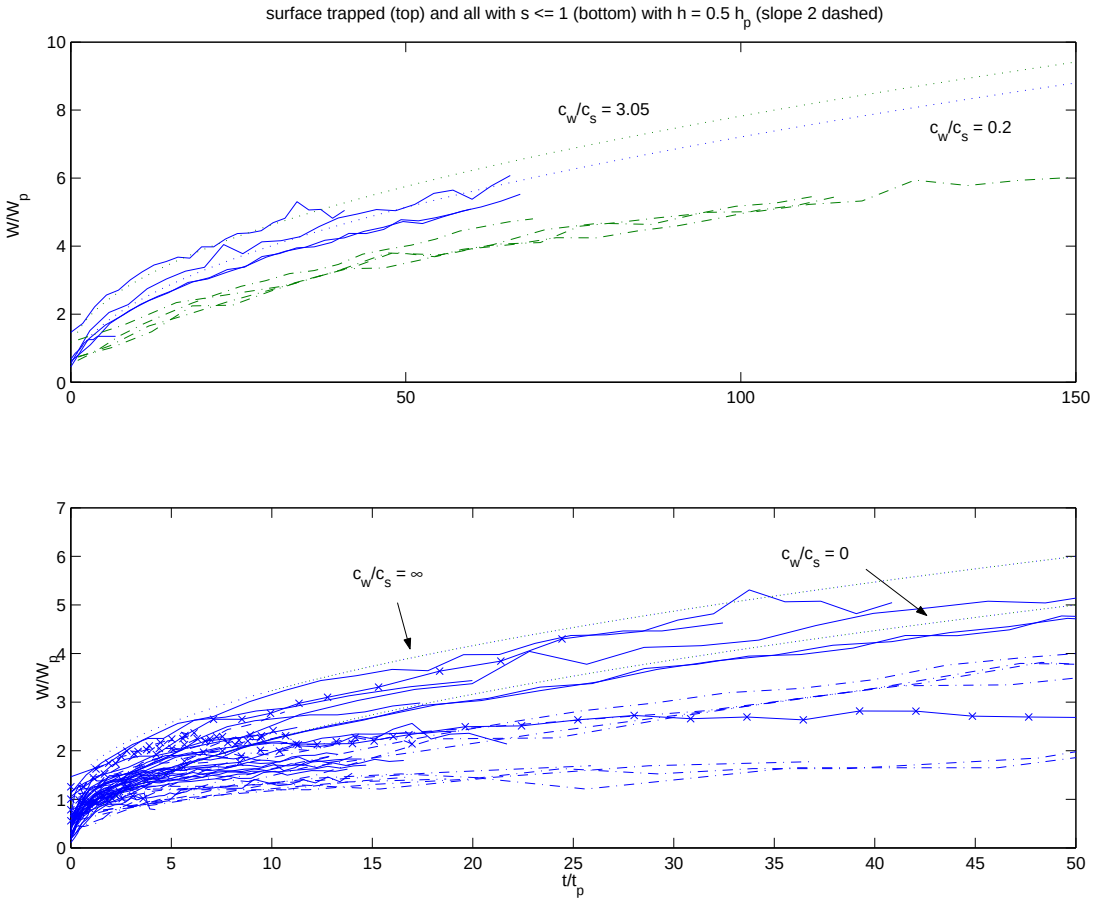

Figure 13: The total width W on slope 1 (solid) and slope 2 (dash-dot) verses time, normalized by the predicted width and time, respectively, assuming $h = h_p/2$. Upper panel: Surface trapped experiments only. Lower panel: All experiments with slope $s < 2$. (Currents with $s > 2$ evolved so quickly that they would not fit on this graph). The experimental measurements should lie between the dotted lines. 'x's indicate that the current is meandering.

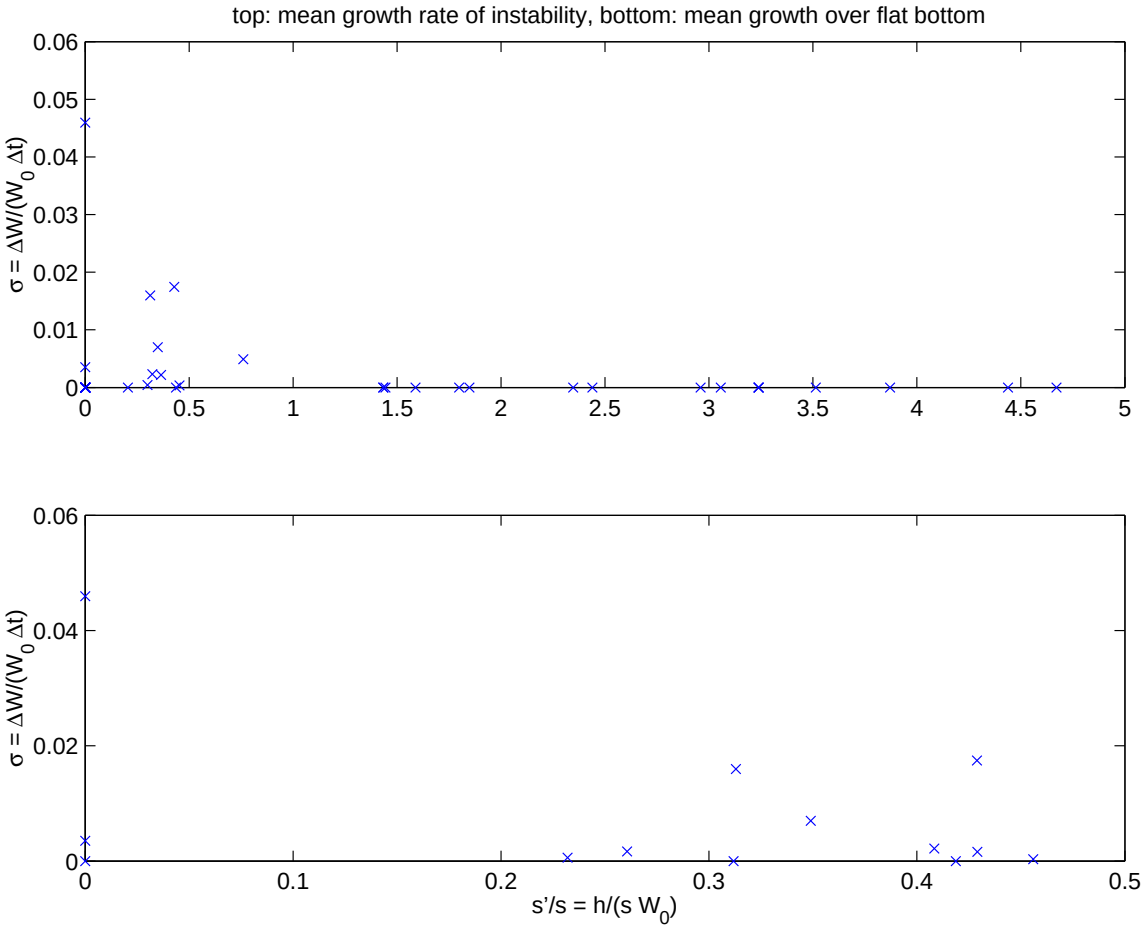

Figure 14: Mean disturbance growth rate as a function of $s'/s < 1$, the ratio of the interface slope to the topographic slope. Upper panel: All experiments. Lower panel: Experiments with $s'/s < 1/2$.

shows how the mean growth rate of disturbances on all currents observed in the experiments depends on the ratio of the interface slope to the topographic slope s'/s. Here we define s' to be the interface slope just before the growth of disturbances. Currents that remained laminar throughout the experiment were defined to have zero disturbance growth. Only those experiments with $s'/s < 1$ showed any disturbance growth, although several experiments with $s'/s < 1$ did *not* show disturbance growth. So $s'/s < 1$ seems to be a necessary, but not sufficient, condition for disturbance growth. The condition $s'/s < 1$ implies that disturbances grow on currents that are predominantly surface trapped and relatively uncoupled to the topography.

6 Conclusion and Discussion

We performed a series of laboratory experiments to investigate the effect of rapid changes in topography on the stability of buoyant coastal currents. It was found that buoyant coastal currents do not form eddies on gentle slopes and do not form eddies on steep slopes until the current width exceeds the shelf width. Eddies formed immediately when the current flowed from a gentle slope to vertical wall. Not only did eddies not form on sloping topography, but eddies generated off the topography were unable to propagate onto the slope. Unstable, eddy-forming currents were immediately stabilized when they flowed onto a gentle slope. Disturbances were able to grow only when the topographic slope exceeded the slope of the frontal interface (i.e. $s'/s < 1$), implying that—for fixed s'—steep slopes are less stable than gentle slopes. This observation is in agreement with some of the conclusions of Reszka and Swaters[10], who state that a steep bottom slope is essential for frontal instability. Our results do not agree, however, with those of Flagg and Beardsley[8] and Gawarkiewicz[9]. Their model fixes the shelf width while the topographic slope is varied, so that increasing the slope also increases the depth of the layer below the front. Given that a two-layer baroclinic instability is most active when the upper and lower layers are of comparable thickness it is not surprising that they should find reduced growth rates at large values of the topographic slope.

The gap experiments demonstrate that gaps which are small compared to the Rossby radius of deformation perturb the flow only weakly and locally. The eddies in our experiments seemed to have a preferred diameter of $\sim 8L_R$ and would not form in the gap until the gap was at least this large. The length of the topographic constriction associated with the formation of Irminger Current eddies is 30–60 L_R[2], which is in the range of the largest gap used in our experiments. We have demonstrated that a topographic gap can generate a large, incoherent eddy field where the eddies tend to accumulate on the downstream edge of the gap. In the Labrador Sea, the background mean flow or β-induced drift would eventually remove the eddies from the gap and inject them into the interior of the Sea. The experiments lacked a background flow and the β effect, so the eddies simply accumulated in the gap.

Viscous effects typically play a much larger role in the laboratory than they do in the ocean, but it difficult to make a quantitative assessment the importance of friction in these experiments. One measure of the impact of viscosity is the barotropic spindown time

$$\tau_{\mathrm{sp}} = \frac{h_p}{\sqrt{\nu f}} = \sqrt{\frac{2Q}{\nu g'}}. \tag{12}$$

For most of the experiments $\tau_{\mathrm{sp}} \approx 50$ s, which is short compared to the length of the experiment and roughly equal to the eddy formation time scale. While easy to calculate and interpret, this time scale is not appropriate for these experiments as the dynamics is clearly baroclinic. A baroclinic spindown time is harder to estimate and depends on the details of the stratification and flow. The baroclinic time scale is longer due to the reduced tendency of a stratified fluid to move as barotropic columns. Until a relevant baroclinic spindown time can be estimated an accurate assessment of the importance of viscosity in these experiments remains elusive.

The topographic slopes used in our experiments are quite large by oceanic standards, as are are the interface slopes. Reasonable oceanic values can be determined by conserving

$$\frac{s'}{s} = \frac{h}{Ls}, \tag{13}$$

the ratio of the relative vorticity in the current to its topographically induced vorticity. For $h = 100$ m and $L = 10$ km we have $s_{\rm oc} \approx 0.05 s_{\rm lab}$. A topographic slope of 0.05 is still quite large, but this is about the order of magnitude of the continental slope off the Mid-Atlantic Bight[9].

7 Acknowledgments

I would like to thank Claudia Cenedese for providing guidance and advice throughout this project, as well as Joe Pedlosky, Karl Helfrich, Dave Chapman, and Steve Lentz for some illuminating discussions. A special thanks to Keith Bradley for providing invaluable assistance in the lab. Finally, I would like to thank all the GFD staff and fellows for providing a wonderful environment for the pursuit of science.

References

[1] J. Lilly, P. Rhines, F. Schott, K. Lavender, J. Lazier, U. Send, and E. D'Asaro, "Observations of the Labrador Sea eddy field," Progress in Oceanography (2003), (Submitted).

[2] C. Katsman, M. Spall, and R. Pickart, "Boundary current eddies and their role in the restratification of the Labrador Sea," J. Phys. Ocean. (2003), (Submitted).

[3] J. Pedlosky, *Geophysical Fluid Dynamics*, 2nd ed. (Springer, ADDRESS, 1987).

[4] J. A. Barth, "Stability of a coastal upwelling front. 1. Model development and stability theorem," J. Geophys. Res. **94**, 10844 (1989).

[5] C. Cenedese and P. Linden, "Stability of a buoyancy-driven coastal current at the shelf break," J. Fluid Mech. **452**, 97 (2002).

[6] S. Condie, "Formation and stability of shelf break fronts," J. Geophys. Res. **98**, 12405 (1993).

[7] J. Whitehead and D. Chapman, "Laboratory observations of a gravity current on a sloping bottom: the generation of shelf waves," J. Fluid Mech. **172**, 373 (1986).

[8] C. Flagg and R. Beardsley, "On the stability of the shelf water/slope water front south of New England," J. Geophys. Res. **83**, 4623 (1978).

[9] G. Gawarkiewicz, "Linear stability models of shelfbreak fronts," J. Phys. Ocean. **21**, 471 (1991).

[10] M. K. Reszka and G. E. Swaters, "Eddy formation and interaction in a baroclinic frontal geostrophic model," J. Phys. Ocean. **29**, 3025 (1999).

[11] A. Bracco and J. Pedlosky, "Vortex generation by topography in locally unstable baroclinic flows," J. Phys. Ocean. **33**, 207 (2003).

[12] R. Samelson and J. Pedlosky, "Local baroclinic instability of flow over variable topography," J. Fluid Mech. 411 (1990).

[13] S. Lentz and K. Helfrich, "Buoyant gravity currents along a sloping bottom in a rotating fluid," J. Fluid Mech. **464**, 251 (2002).

[14] D. Chapman and S. Lentz, "Trapping of a coastal density front by the bottom boundary layer," J. Phys. Ocean. 1464 (1994).

[15] A. Yankovsky and D. Chapman, "A simple theory for the fate of buoyant coastal discharges," J. Phys. Ocean. **27**, 1386 (1997).